Acta Crystallographica Section B
Structural Science
ISSN 0108-7681

Inversion of 4*f*-states in CeB_6 thermally excited at 430 K

Ryoko Makita,[a]* Kiyoaki Tanaka,[a] Yoshichika Ōnuki[b] and Hiroshi Tatewaki[c]

[a]Graduate School of Materials Science and Engineering, Nagoya Institute of Technology, Japan, [b]Graduate School of Science, Osaka University, Japan, and [c]Graduate School of Natural Science, Nagoya City University, Japan

Correspondence e-mail: 14515020@stn.nitech.ac.jp

Received 24 January 2007
Accepted 18 July 2007

The 4*f* states of Ce in a typical Kondo crystal, CeB_6, are split into an excited state Γ_7 and the ground state Γ_8, with an excitation energy at 560 K. The electron-density distribution of the thermally excited state was measured at 430 K using a four-circle diffractometer equipped with a small furnace. In contrast to the previous results at lower temperature, electrons are transferred from B_6 to Ce at 430 K. X-ray atomic-orbital analysis revealed that the 5*d*-Γ_8 orbitals (the energy level of which is similar to that of the B-2*p* orbitals) are fully occupied and the 4*f*-Γ_7 orbitals are more populated than the 4*f*-Γ_8 orbitals. Fully occupied 5*d*-Γ_8 makes the 4*f*-Γ_8 states unstable and the energy levels of 4*f*-Γ_7 and 4*f*-Γ_8 are inverted.

1. Introduction

The observation and quantitative analysis of electron-density distributions (EDD) in crystals with heavy atoms such as rare-earth elements still remain very difficult. Further, analysis has recently become more and more important because of the many interesting rare-earth crystals, including high-temperature superconductors. The 4*f*-EDD in the difference density map in CeB_6 was observed by Sato (1985) and it was attributed to the electrons in the $4f(j = 5/2)\Gamma_8$ orbitals. The 4*f*-EDD was measured again at 165 K (Tanaka *et al.*, 1997) and analyzed using the real 4*f* atomic orbitals (AO; Weiss & Freeman, 1959). The peaks in the deformation density map around Ce with a height of 2.0 e $Å^{-3}$ were reduced to 0.2 e $Å^{-3}$ by the analysis at 165 K. The temperature dependence of the EDD of CeB_6 was further measured at 100, 165, 230 and 298 K and was analyzed using an X-ray atomic orbital analysis (XAO; Tanaka & Ōnuki, 2002). The analysis showed that the 4*f*-electrons are transferred from Ce to the B_6 moiety as temperature is decreased. The residual densities around Ce at the four temperatures showed excellent agreement. The quantitative analysis of 4*f*-EDD was also investigated by Claiser *et al.* (2004) in the gadolinium–semiquinone complex. They carried out multipole refinement and compared the results calculated with six types of form factors. Consequently, the EDD of the organic ligands showed excellent agreement, however, the residual density peak around Gd remains ~ 1 e $Å^{-3}$.

The EDD observation of excited states is a rarely explored field. Several investigations concerning the excited states ($4d^9 4f^{n+1}$) of CeB_6 were performed by means of photoelectron spectroscopy (Ichikawa *et al.*, 1986; Kakizaki *et al.*, 1995). In a field of X-ray diffraction Pressprich *et al.* (1994) succeeded in measuring the static deformation density of the metastable electronic excited state of sodium nitroprusside. Furthermore, Kim *et al.* (2002) determined the structure of the

photo-induced excited state of $[Pt_2(pop)_4]^{4-}$ ion [pop = pyrophosphate, $(H_2P_2O_5)^{2-}$] by time-resolved X-ray diffraction. Ozawa *et al.* (2003) also observed the EDD of a photo-excited diplatium complex using a low-temperature vacuum X-ray camera. In the present study electron transfer among thermally excited states was observed. Although the experiments of the photo-excited crystals can now determine the structures of molecules in the excited state with very short lifetimes, the final aim of the photo-excited crystallography seems to identify the electronic states related to the excitation process by X-ray EDD analysis. The present study, in which electron transfer was observed among atomic orbitals identified by the X-ray EDD analysis, forms one of the bases of the future crystallography of excited states. X-ray diffraction has now become a tool for not only analysing the structure, but also observing the process involved in the transition from the ground state to excited states, just like spectroscopy.

CeB_6 is one of the most important complexes of the heavy-fermion system and has been investigated extensively at low temperatures owing to its many interesting properties, such as competition between the Kondo effect and the RKKY interaction, and antiferro-quadropolar ordering. CeB_6 has a CsCl-type structure (space group, $Pm\bar{3}m$). There are regular B_6 octahedra at the corners of the unit cell with Ce at the body-centre of the cubic unit cell. Ce^{3+} formally has one 4*f* electron. When spin-orbital interactions are taken into account, the 4*f* orbitals split into two 4*f* states with $j = 5/2$ and $j = 7/2$. Since the energy of the latter is higher, the 4*f* orbitals with $j = 7/2$ were not found to be occupied in the present study. In the O_h crystal field, $4f(j = 5/2)$ orbitals are further split into two orbitals: the excited states Γ_7 (doublet) and the ground states Γ_8 (quartet). The excitation energy between Γ_7 and Γ_8 was reported to be 530–560 K (Loewenhaupt *et al.*, 1985; Zirngiebl *et al.*, 1984). In the present study, temperature T is used as the expression of energy instead of using kT (K: Boltzmann constant). When Boltzmann statistics are assumed, the ratio of the electron poplulations of the two states is expressed as

$$n(\Gamma_7)/n(\Gamma_8) = \exp(-\Delta E/kT), \quad (1)$$

where ΔE is an excitation energy. Assuming $\Delta E = 560$ K, the ratio of Γ_7:Γ_8 populations at 430 K becomes 0.27.

In the previous study (Tanaka & Ōnuki, 2002), significant numbers of electrons were observed in the excited Γ_7 orbitals of CeB_6 at 298 K, with the $n(\Gamma_7)/n(\Gamma_8)$ ratio equal to 0.10. As temperature increases this ratio may increase, as expected from (1). Therefore, the first aim of the present study is to confirm the existence of electrons in the excited Γ_7 orbitals and to observe the EDD of the excited states of CeB_6 at 430 K,[1] which was selected because it is central between 560 K and room temperature. The second aim is to develop the method to measure EDD accurately at high temperature. The third aim is to demonstrate how well the XAO analysis (in which atoms are divided into sub-shell electrons and each sub-shell is treated as an independent atom) works for these heavy-atom systems (Tanaka, 1988; Tanaka & Ōnuki, 2002).

2. Experimental

A CeB_6 single crystal was heated up to 430 K in a furnace installed on the diffractometer. The furnace was designed according to a previous study by Kodama (1984), which was originally designed based on a study by Ishizawa & Kato (1983). The furnace on an X-Y-Z stage equipped with a brass cylinder containing a spiral Pt wire was mounted on the χ-circle of the diffractometer, as illustrated in Fig. 1. N_2 gas was passed through a Pt coil to heat the crystal. To have a wider and stable equi-temperature area Pt wire was extended around the crystal, as proposed by Brown *et al.* (1973). The N_2-gas flow rate was kept constant using a flowmeter (KOFLOC 8300). A transformer (Aihara Electric Co., Ltd SD-1110) was used to keep the circuit voltage constant. Pt wire was also incorporated into the circuit to allow the voltage to the Pt heater to change continuously. After placing the Pt–13%Rh thermocouple at the crystal position the furnace was adjusted by the X-Y-Z stage so that temperature reaches the maximum. The relationships between the current in the Pt heater and the temperature of the sample were measured at $\chi = 0^\circ$ on a four-circle diffratometer using the crystals, naphthalene, phthalic anhydride, Sn, NH_4NO_3 and $NaNO_3$ with melting points of 353, 401, 505, 443 and 580 K, respectively. A thermocouple was placed at the crystal-position temperature at fixed currents between 2 and 6 A at $\chi = 0$ and $\chi = 90^\circ$. Temperatures at $\chi = 0^\circ$ agree with the calibration curve, but those at $\chi = 90^\circ$ do not. Hence, the temperature variation with χ angles was measured, keeping an electric current in the Pt wire at 3.8 A, which kept the crystal approximately at 430 K. A CeB_6 crystal on the goniometer was covered by a Kapton film of 25 µm thick (Du Pont-Toray) and the temperature of the crystal was

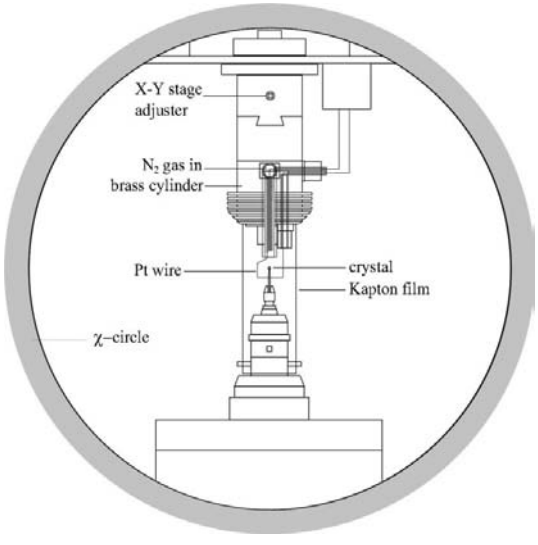

Figure 1
Equipment for accurate high-temperature X-ray intensity measurement.

[1] The occupied $4f(j = 5/2)\Gamma_8$ states consist of the ground state and $4f(j = 5/2)\Gamma_7$ is the excited state below room temperature. At 430 K more drastic change occurs in CeB_6 and the Γ_7 states cannot be called the excited states.

Table 1
Crystal data of CeB_6 at 430 K.

Crystal data	
Chemical formula	$B_6^{3-}\cdot Ce^{3+}$
M_r	204.98
Cell setting, space group	Cubic, $Pm\bar{3}m$
Temperature (K)	430.0 (5)
a (Å)	4.14586 (8)
V (Å^3)	71.26 (1)
Z	1
D_x (Mg m^{-3})	4.777
Radiation type	Mo $K\alpha$
μ (mm^{-1})	15.63
Crystal form, colour	Sphere, metallic dark purple
Crystal radius (mm)	0.037
Data collection	
Diffractometer	Four-circle (MAC SCIENCE)
Data collection method	Integrated intensities data fom $\omega/2\theta$ scans
Scan speed in ω (min^{-1})	2
Maximum no. of scans	10
Absorption correction	For a sphere
T_{min}	0.435
T_{max}	0.482
No. of measured, independent and observed reflections	990, 181, 170
Criterion for observed reflections	$F > 3.0\sigma(F)$
R_{int}	0.063
θ_{max} (°)	74.2
No. and frequency of standard reflections	3 every 50 reflections
Refinement	
Refinement on	F
$R[F^2> 2\sigma(F^2)]$, $wR(F^2)$, S	0.012, 0.015, 1.14
No. of reflections	702
No. of parameters	38
H-atom treatment	No H atoms present
Weighting scheme	Based on measured s.u.'s
$(\Delta/\sigma)_{max}$	0.001
$\Delta\rho_{max}$, $\Delta\rho_{min}$ (e Å^{-3})	0.57, −0.70
Extinction method	B-C type 1 Gaussian anisotropic
Extinction coefficient	0.334 (3) × 10^4

Computer programs used: *IUANGLE* (Tanaka *et al.*, 1994); RSLC-3 *UNICS* system (Sakurai & Kobayashi, 1979).

kept at 430 ± 2.5 K, limiting the χ angle between −60 and 50°. The furnace allows the ω angle to rotate from −53 to 65°.

A CeB_6 single crystal was shaped into a sphere with a radius of 37 µm. This crystal was glued to a glass rod 30 µm in diameter by Aron Ceramic D (Toagosei). After heating the crystal for 1 h to stabilize the temperature, measurements were then taken. The orientation matrix and lattice parameter were determined by reflections 155 and 633 with 2θ around 75°, where the peaks due to $K\alpha_1$ and $K\alpha_2$ radiations were well separated. X-ray intensities were measured using a four-circle diffractometer (MAC Science). CeB_6 has 88 electrons in the unit cell, formally including only one $4f$ electron. Since the multiple diffraction effect easily exceeds 1% of the structure factors, as shown in Fig. 2 of our previous paper (Tanaka & Ōnuki, 2002) and in PtP_2 (Tanaka *et al.*, 1994), good results were never expected without avoiding or correcting for the multiple diffraction in the investigation of the EDD of heavy-atom crystals. Since the multiple diffraction effect is very sensitive to the orientation of the crystal and width of the Bragg peak, it is better to avoid it by rotating the crystal around the scattering vector (ψ rotation). Most of the reflections have secondary reflections, part or all of which are on the reflection sphere at the same time as when the reflection is being measured. The optimum ψ angle at which multiple diffraction contributed less than 0.25% to each structure factor was calculated with the program *IUANGLE* (Tanaka *et al.*, 1994) after the orientation of the crystal was determined.

The furnace and the avoidance of multiple diffraction decreased the possible area for intensity measurement. The definition of the possible area was defined in the program *IUANGLE*, but an unexpected shadow area still remained. The Pt wire around the crystal, which is necessary to have a wider and stable equi-temperature area, often scatters X-rays or interrupts incident and diffracted X-rays in the present experiment, and some of the significant reflections were rejected based on the following reasons. There were 20 reflections with $F < 3\sigma F$ which were rejected among the 990 measured reflections and 84 reflections whose peak profiles were partial when the difference between 2θ and ω was $\sim 65 \pm 5°$. The R_{int} value for 886 (990–84–20) reflections was 0.0136, indicating the very severe shadowing effect of the Pt wire. There were 91 reflections with an anomalous background caused by the scattering of the incident beam by the Pt wire. There were 80 reflections with $\sin\theta/\lambda$ more than 1.34 ($2\theta \geq 145°$), which were rejected because of the high background owing to the air scattering of the incident X-rays. Among the reflections with more than three equivalent reflections 12 were rejected because of too much deviation from the mean of the equivalent reflections, for unknown reasons. One reflection was rejected because of unavoidable multiple diffraction. Hence, 288 reflections were rejected and 702 reflections remained. The R_{int}(990) and R_{int}(702) values were 0.0629 and 0.0095, respectively. The number of independent reflections whose 2θ value is more than 145° is 6. The number of independent reflections from 990 measured reflections and 702 used reflections in the 2θ range less than 145° are 175 and 170; the completeness values are 94.1 and 91.4%, respectively. These rejected reflections may enhance the series termination effect in the residual densities, as stated in the previous study (Tanaka & Ōnuki, 2002). However, that does not significantly alter the result of the analysis, which will be mentioned in §5. Other data collection details are summarized in Table 1.[2]

3. Refinement

The reflection data were refined by the least-squares program *QNTAO* (Tanaka & Ōnuki, 2002; Tanaka *et al.*, 2007). The valences of Ce and B were initially assumed to be +3 and −0.5, respectively. A spin-orbit interaction was assumed for Ce and the scattering factor was calculated using the program *SFRSCF* (Tanaka *et al.*, 2007). This calculation of relativistic atomic orbitals was carried out by Hitoshi Tatewaki using the

[2] Supplementary data for this paper are available from the IUCr electronic archives (Reference: OG5021). Services for accessing these data are described at the back of the journal.

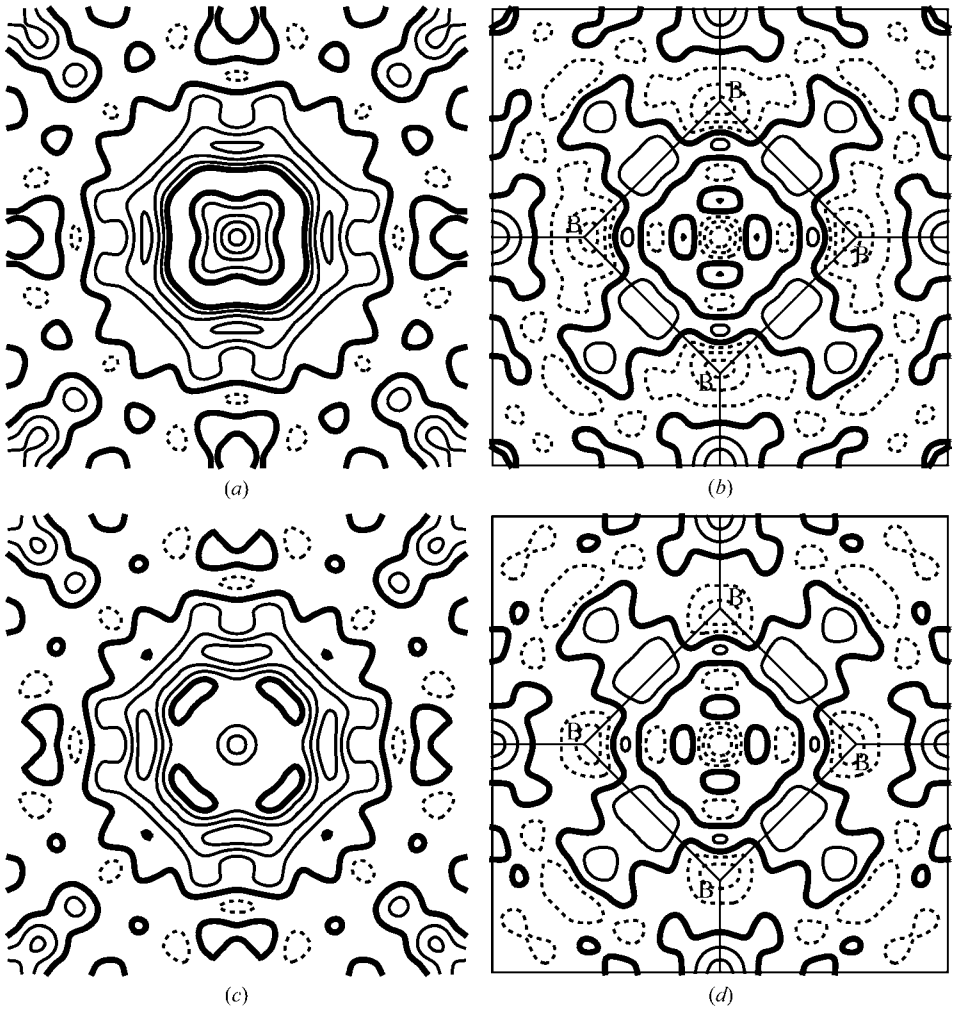

Figure 2
Difference densities (*a*) around Ce at $(\frac{1}{2},\frac{1}{2},\frac{1}{2})$ on the plane 100, (*b*) around B after the refinement (A), (*c*) around Ce and (*d*) around B after the refinement (B). Contours are at intervals of 0.2 e Å^{-3}. Zero contours are drawn as thick lines, positive contours as thin lines, and negative contour as broken lines.

program *GRASP* (Dyall *et al.*, 1989). The scattering factors of B were calculated based on the self-consistent field (SCF) wavefunction (Mann, 1968). Anomalous dispersion terms of the atoms were taken from *International Tables for X-ray Crystallography* (1992, Vol. C). Extinction parameters are assumed to be type I with a Thornley–Nelmes distribution function (Thornley & Nelmes, 1974; Becker & Coppens, 1974*a*,*b*, 1975). Analysis is basically divided into three stages. The parameters refined in the previous stage were also shifted in the next stage.

The first stage was the spherical-atom refinement. We assumed that electrons were configured equally to each subshell orbital, which makes the spherical EDD. In this stage, the scale factors, the atomic coordinate z of B, the harmonic temperature factors and the extinction parameters were refined. The second stage is the refinement of the anharmonic vibration (AHV). In this stage, the AHV parameters were refined in addition to those of the first-stage fixing harmonic temperature factors. The harmonic and anharmonic parameters were refined by alternately fixing the other factors, but the parameters of the AHV could not be refined with the parameters for AOs. The third stage is the XAO analysis. In this stage, electron populations and κ parameters (Coppens *et al.*, 1979), which represent the expansion–contraction of each orbital, are refined in addition to the parameters of the first stage.

3.1. Anharmonic vibration

Dawson *et al.* (1967) proposed the treatment of temperature factors including the anharmonic thermal vibration effect for high-symmetry crystals by means of series expansion of the one-particle potential. Tanaka & Marumo (1983) generalized the treatment, and anharmonic third and fourth-order parameters are refined with *QNTAO*. The method was used because it is formulated based on the vibration of the atoms around their equilibrium positions, which makes it more difficult to include aspherical EDD due to electron configuration itself rather than the other statistical methods. AHV parameters are restricted by the site symmetry of Ce($m\bar{3}m$) and B($\bar{4}mm$) and the anharmonic potential V of each atom is represented by the following equation

$$\begin{aligned} V_{\rm Ce} &= q_{1111}(u_1^4+u_2^4+u_3^4)+q_{1122}(u_1^2u_2^2+u_1^2u_3^2+u_2^2u_3^2)\\ V_{\rm B} &= c_{111}(u_1^3+u_2^3)+c_{333}u_3^3+q_{1111}(u_1^4+u_2^4)\\ &\quad +q_{3333}u_3^4+q_{1122}u_1^2u_2^2+q_{1133}(u_1^2u_3^2+u_2^2u_3^2), \end{aligned} \qquad (2)$$

where $\mathbf{u} = (u_1,u_2,u_3)$ is a displacement vector from the equilibrium position of each atom defined on the coordinate system with axes parallel to the crystal axes, $\boldsymbol{a}$, $\boldsymbol{b}$ and $\boldsymbol{c}$. Since AHV parameters are closely related to high-angle reflections, 4*f* electrons located near the inner shell are expected to be strongly affected by AHV. However, AHV parameters are not significant in the present study, as stated in §3.2. In the previous study (Tanaka & Ōnuki, 2002), a significant shift of the z coordinate was observed when the anharmonic cubic parameters were refined with the z coordinate. However, such a shift was not observed, regardless of whether anharmonic cubic parameters are refined with the z coordinate or not. This

Table 2
Extinction and final parameters.

Parameters given: Parameters for B at (0,0,*z*). Electron populations *n*, κ parameter, anisotropic temperature factors U^{ij} ($\times 10^{-5}$ Å^2), harmonic b_i ($\times 10^{-21}$ J Å^{-2}), anharmonic cubic parameters c_{ijj} ($\times 10^{-19}$ J Å^{-3}), quartic parameters q_{iijj} ($\times 10^{-19}$ J Å^{-4}). Degeneracy of each orbital is shown in the parentheses after *n*. Anisotropic temperature factors are defined as $T_H = \exp(-2\pi^2 \sum_{i,j} h_i h_j a_i^* a_j^* U^{ij})$ and anharmonic potentials *V* are defined in the text. *R* factors: $R_1 = \Sigma||F_o| - |F_c||/\Sigma|F_o|$, $R_2 = \Sigma(|F_o| - |F_c|)^2/\Sigma|F_o|^2$. Anisotropic type I extinction parameters with Thornley–Nelmes distribution function. Parameter after (A). Spherical-atom analysis before AHV analysis, (B). XAO analysis without 5*d* orbitals, (C). XAO analysis including 5*d*(*j* = 5/2) orbitals, (D). XAO analysis including 5*d*(*j* = 3/2) orbitals.

Refinement	(A)	(B)	(C)	(D)
R_1	0.001253	0.001216	0.001157	0.001162
R_2	0.001685	0.001637	0.001498	0.001511
Ce				
U^{11}	850 (2)	847 (1)	843 (1)	843 (1)
b_1	698 (2)	701 (1)	704 (1)	704 (1)
n (4*f j* = 5/2 Γ_8)(4)	1/6	0.06 (3)	0.06 (2)	0.07 (3)
n (4*f* = 5/2 Γ_7)(2)	1/6	0.36 (11)	0.37 (11)	0.26 (9)
n (5*p j* = 3/2)(4)	1.00	1.00	1.00	1.00
n (5*p j* = 1/2)(2)	1.00	1.00	1.00	1.00
n (5*d j* = 5/2 Γ_8)(4)	–	–	1.00	–
n (5*d j* = 5/2 Γ_7)(2)	–	–	0.00	–
n (5*d j* = 3/2)(4)	–	–	–	1.00
κ (4*f j* = 5/2 Γ_8)	–	1.19 (40)	1.29 (22)	1.26 (19)
κ (4*f j* = 5/2 Γ_7)	–	1.05 (18)	1.07 (20)	1.13 (19)
κ (5*p j* = 3/2)	–	1.00	0.86 (14)	0.89 (5)
κ (5*p j* = 1/2)	1.00	1.00	1.00	1.00
κ (5*d j* = 5/2 Γ_8)	–	–	1.13 (16)	–
κ (5*d j* = 5/2 Γ_7)	–	–	–	–
κ (5*d j* = 3/2)	–	–	–	1.08 (8)
q_{1111}	0.0	−0.04 (24)	−0.03 (24)	−0.03 (24)
q_{1122}	0.0	−0.8 (7)	−0.7 (7)	−0.7 (7)
B				
z	0.30084 (29)	0.30084 (29)	0.30085 (14)	0.30081 (14)
U^{11}	611 (9)	612 (8)	607 (8)	607 (8)
U^{33}	374 (12)	374 (13)	370 (12)	371 (12)
b_1	971 (14)	970 (13)	979 (13)	979 (12)
b_3	1589 (51)	1589 (53)	1605 (53)	1600 (53)
n (2*s*)(1)	2.00	2.00	2.00	2.00
n (2p_x) = *n* (2p_y)(2)	1/2	0.41 (11)	0.10 (6)	0.14 (6)
n (2p_z)(1)	1/2	0.63 (23)	0.63 (13)	0.60 (13)
κ (2*s*)	–	1.01 (4)	0.99 (6)	1.00 (4)
κ (2p_x) = κ (2p_y)	–	0.71 (23)	0.90 (66)	0.89 (62)
κ (2p_z)	–	0.93 (19)	0.93 (14)	0.93 (17)
c_{311}	0.0	−0.6 (10)	−0.6 (10)	−0.6 (10)
c_{333}	0.0	0.5 (10)	0.4 (10)	0.4 (10)
q_{1111}	0.0	0.1 (40)	0.1 (40)	0.1 (40)
q_{3333}	0.0	−11 (12)	−11 (12)	−11 (12)
q_{1122}	0.0	−29 (23)	−28 (23)	−28 (23)
q_{1133}	0.0	29 (24)	29 (24)	29 (24)
Extinction				
Y_{11}	9.4 (4)	8.7 (3)	9.0 (4)	9.3 (5)
Y_{22}	5.9 (8)	6.0 (7)	7.4 (9)	7.0 (9)
Y_{33}	10.6 (8)	10.2 (8)	11.3 (8)	11.0 (9)
Y_{12}	−0.7 (4)	−0.8 (4)	−1.1 (4)	−1.0 (4)
Y_{13}	0.9 (4)	0.8 (3)	0.5 (3)	0.6 (3)
Y_{23}	1.1 (7)	1.4 (6)	1.4 (6)	1.5 (6)

is because the anharmonic parameter c_{333} is not significant. The parameters of AHV could not be refined with the orbital parameters discussed in the next section.

3.2. XAO analysis

We refined the diffraction data by means of the method which we call the XAO analysis. Electron density was divided into those of the core and of the valence electrons and the latter are further divided into those of the various subshell electrons, which enables us to treat localized electron density quantitatively. The sub-shell orbitals were constrained to be strictly orthonormal to one another. The XAO analysis is based on the quantum-mechanical orbital models and is useful for investigations of ionic crystals and heavy-atom crystals. In these investigations localized *d* or *f* electrons play an important role in determining the physical properties of materials. The contribution of two-centre electrons in the covalent or coordination bonds, which appear in molecular orbital (MO) models, to structure factors is not significant. The details of the method will be reported elsewhere (Tanaka *et al.*, 2007).

In the present study 4*f*(*j* = 5/2), 5*p*(*j* = 3/2), 5*p*(*j* = 1/2) of Ce and 2*s*, 2*p* of B were assumed as the valence sub-shells. The electroneutrality of the crystal was maintained during the refinement by making the total sum of the electron populations of the sub-shell orbitals equal to that of the positive charges of nuclei in the unit cell. In the present study the following equation was applied

$$\begin{aligned} &g_{\rm Ce}[4n(4f_{j=5/2}\Gamma_8) + 2n(4f_{j=5/2}\Gamma_7) + 4n(5p_{j=3/2}) \\ &+ 2n(5p_{j=1/2}) + 48] + g_{\rm B}[2n(2p_x) + n(2p_z) + n(2s) + 2] \\ &= g_{\rm Ce}Z_{\rm Ce} + g_{\rm B}Z_{\rm B}, \end{aligned} \tag{3}$$

where *g*, *n* and *Z* are the multiplicities of Ce and B in the unit cell of atomic sites, electron population and atomic number, respectively. The numbers in front of the electron populations are the degeneracy of each orbital imposed by the crystal symmetry; the orbitals are specified in parentheses. The above restriction reduces the number of independent parameters in the least-squares refinement by one. In the present study the parameters of the electron populations are considered to be independent, except $n(2p_z)$. When the population parameters are determined, $n(2p_z)$ is also determined according to (3). Equation (3) enables us to analyze electron transfer between atoms in the crystal. Moreover, it permits us to treat the EDD of non-stoichiometric compounds such as solid solutions and metals. When a quantization axis *z* is taken along *c* for B, the point-group symmetry constraints $n(2p_x)$ and $n(2p_y)$ are the same. The same constraint was also imposed on the κ parameters. In the present study, the quantization axes were taken parallel to the crystal axes.

After AHV parameters were refined, they were fixed and electron populations *n* were added in the refinement. Then κ parameters were refined. The electron populations were refined under the constraint that *n* is greater than 0, or less than 2 or 1 for AOs of B and Ce, respectively. When one exceeded the limit, it was kept to the limiting value and the parameter was excluded from the refinement to avoid parameter correlations. At each step of the refinement the residual density was examined carefully to assess the validity of the parameters in the refinement and identify the parameters to be added in the next stage. Thus, the Ce-4*f* orbitals were refined first and then the Ce-5*d* orbitals were added to explain the residual density, as will be discussed in the next section.

In the refinement, although orthonormal constraints among orbitals are strictly obeyed and the values of the correlation coefficients are not greater than 0.5, large parameter interactions are found. For example, between the electron population and extinction parameters, κ parameters of Ce-4*f* and extinction parameters, electron populations of Ce-4*f* and κ parameters of B-2*p*, and scale factors and κ parameters. When we attempted to refine these parameters simultaneously, variations of these values were too large and peaks in residual density around Ce became higher. Hence they were refined separately. Parameter interaction at each stage of the refinement will be discussed in the next section. Since the electron population of $n(5p_{j=3/2})$, $n(5p_{j=1/2})$ and $n(2s)$ tended to exceed full occupation, they were also fixed at 1.0, 1.0 and 2.0, respectively. B-2*s* is always fully occupied as in the previous refinement (Tanaka & Ōnuki, 2002). Since the residual density around Ce became larger when the κ parameter of Ce-$5p_{j=3/2}$ was refined, it was also fixed to 1.0. This corresponds to assuming Ce-$5p_{j=3/2}$ to be one of the core orbitals. Although there is a strong correlation between electron populations and extinction parameters, they converged well. The AHV parameters, except q_{1122} of Ce and B, and q_{1133} of B, were not significant, although temperature is high.

4. Result and discussion

4.1. Spherical-atom model

When scattering factors evaluated from relativistic AOs calculated by the program *GRASP* (Dyall *et al.*, 1989) were used, there were less parameter interactions than using the AOs calculated with the program *HEX* by Liberman *et al.* (1971), which were employed in the previous study (Tanaka & Ōnuki, 2002). Residual densities and *R* factors also became slightly better but there is no essential difference in the EDD.

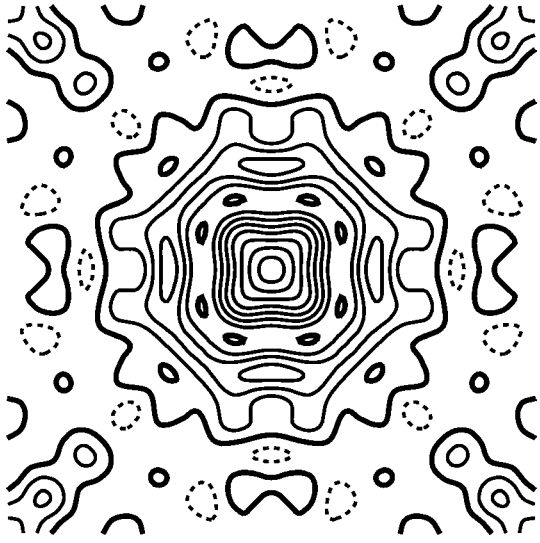

Figure 3
Sum of the EDD of Ce-Γ_7 orbitals (see text). Contours are as Fig. 2.

The parameters after the spherical-atom refinement (refinement A) are listed in Table 2 and the difference densities around Ce^{3+} and $B^{0.5-}$ are shown in Figs. 2(*a*) and (*b*), respectively. From Fig. 2(*a*), the positive peak on Ce extends along the ⟨110⟩ direction corresponding to the Γ_7 orbitals. The anisotropic temperature factors of Ce are larger than those of B. According to the previous study (Tanaka & Ōnuki, 2002), at low temperatures the U^{11} value of Ce is smaller than that of B, but the order is reversed at higher temperature. The anisotropic temperature factors of Ce and B increase proportionally with temperature from 100 to 430 K, but U^{11} of Ce increases more than the U^{ij} parameters of B. This may be due to the strong covalent bonds connecting the B_6 octahedra throughout the crystal. A fully occupied B-2*s* orbital also contributes to make a strong $2p\sigma$ orbital. B atoms were fixed more firmly than the Ce atom, which is located at the relatively free centre of the unit cell. The bond lengths of $B-B_{out}$, which is the B—B bond connecting two B_6 octahedra, and $B-B_{in}$, which is the B—B bond within B_6 octahedra, are 1.6513 (6) and 1.7640 (4) Å, respectively. The difference density on the $B-B_{out}$ bond between B_6 octahedra in Fig. 2(*b*) is twice those on the $B-B_{in}$ bonds within the B_6 octahedron. This is consistent with the fact that $B-B_{out}$ is a stronger bond than $B-B_{in}$ judging from the bond length.

4.2. AHV and XAO analysis

4.2.1. Thermal excitation. Parameters from the XAO analysis without Ce-5*d* orbitals (refinement B), which includes AHV analysis, are also listed in Table 2 and the residual densities around Ce and B are shown in Figs. 2(*c*) and (*d*). The peaks around Ce in Fig. 2(*a*) mentioned in §4.1 corresponded to $n(4f_{j=5/2}\Gamma_7)$, which is greater than 1/6. These peaks disappear in Fig. 2(*c*), supporting the fact that significant populations exist in $4f(j = 5/2)$ orbitals; the population inversion between $4f(j = 5/2)\Gamma_8$ and Γ_7 orbitals is also supported. At room temperature the Γ_8 orbital is more populated. Fig. 3 is the EDD of the excited 4*f*-Γ_7 orbitals calculated as a Fourier transform of the differences between observed structure factors and those calculated without the Γ_7 electrons. Therefore, the Ce peak extending along ⟨110⟩ in Fig. 3 corresponds to the sum of the EDD of the Γ_7 orbitals. Since the B-$2p_z$ orbital extends along the edge of the cubic unit cell and contributes mainly to the $B-B_{out}$ bonds, larger $n(2p_z)$ than $n(2p_x)$ also explains the residual density in Fig. 2(*b*), where the edge centres (central part of the $B-B_{out}$ bonds) have the highest peaks. Since the MO model is not used in the present study, the residual density on the $B-B_{out}$ covalent bond in Fig. 2(*d*) is not improved except for the reduced hole at the B atom. The XAO analysis does not explain the bonding electrons in the centre of the B—B covalent bonds, which are mainly due to the two-centre electrons in an MO model. The MO model should be employed to analyze the EDD in and between the B_6 octahedra. Since the melting point of CeB_6 is 2550 K and CeB_6 has a high hardness, even at high temperature, most of the AHV parameters are not significant. This means that the aspherical bonding features are not explained

by AHV either. At 100 and 165 K AHV is significant, where electron transfer from Ce to $B-B_{out}$ bonds changes the charge valence in the unit cell dramatically and AHV is enhanced (Tanaka & Ōnuki, 2002). However, in the present study electrons are back-donated from B_6 to Ce and the crystal field of B_6 is weaker. This is expected to be another reason why AHV is not significant at 430 K.

4.2.2. Contribution of 5*d* orbitals. In order to investigate the inversion of the populations on $4f$-Γ_8 and $4f$-Γ_7 (which indicate that the energy levels of the two orbitals are inverted) and to find the origin of the peaks of 0.6 e Å^{-3} along the ⟨100⟩ direction of residual density at 0.8 Å from Ce in Figs. 2(*a*) and (*c*), further refinements were required. Thus, the contribution of the 5*d* orbitals of Ce to the peaks was taken into account, although 5*d* orbitals were not occupied when X-ray diffraction data at 298 K (measured by Tanaka & Ōnuki, 2002) were analyzed. The energy level of the 5*d* orbitals estimated by spectroscopy was much higher than that of the 4*f* orbitals (Martin *et al.*, 1978). However, according to the band structure of CeB_6, 4*f* bands are hybridized with a 5*d* band around the Fermi energy (Heide *et al.*, 1986). The Fermi surface of CeB_6 centred at the X point in the Brillouin zone, which corresponds to the edge centres, exhibits the hybridized character of the Ce-5*d* and B-2*p* states (Souma *et al.*, 2004). Therefore, we attempted to include the 5*d* orbitals in the outer shell. A schematic drawing of the energy levels of B and Ce is shown in Fig. 4(*a*). The 5*d* orbitals split into those with $j = 5/2$ and 3/2 because of spin-orbit interactions. The $5d(j = 5/2)$ orbitals split further into the two orbitals Γ_7 (doublet) and Γ_8 (quartet) in the O_h crystal field. The Γ_8 orbitals are more stable than the Γ_7 orbitals. Note that the energy of $5d(j = 3/2)$ orbitals is higher than that of $5d(j = 5/2)$ orbitals. This is because the present

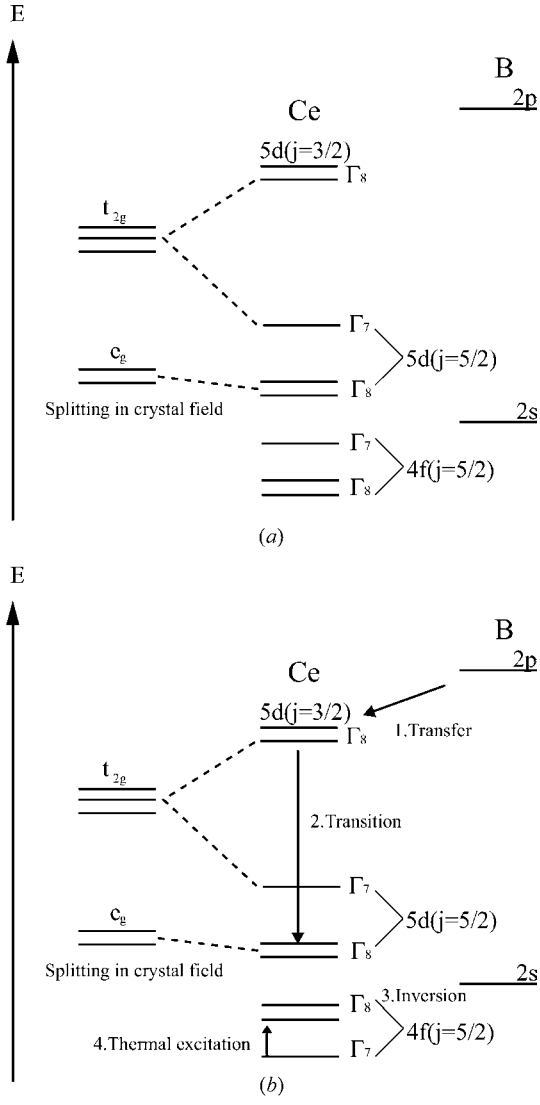

Figure 4
Schematic drawing of the energy levels of Ce and B, (*a*) below room temperature and (*b*) at 430 K. The energy levels of Ce are estimated using the program *HEX* (Liberman *et al.*, 1971); those of B are calculated by Mann (1968).

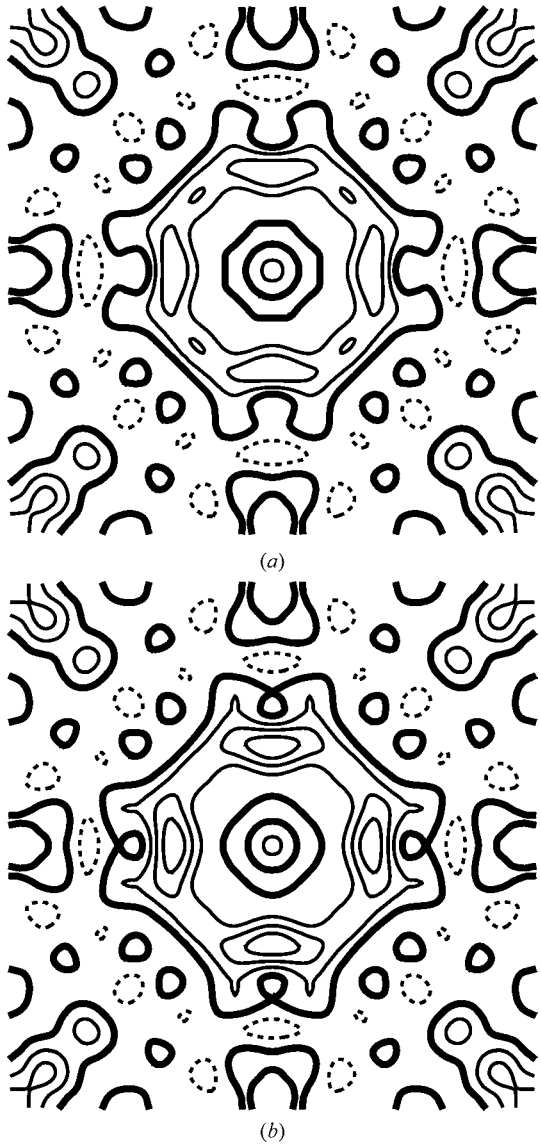

Figure 5
Residual densities around Ce (*a*) after refinement (C) and (*b*) after refinement (D). Contours are as Fig. 2.

quantization axes are directed along the ⟨100⟩ direction or to the vacant face-centres of the cubic cell. The energy levels of e_g orbitals, which have the electron lobe along the quantization axes, are lower than those of t_{2g} orbitals. Hence the energy of $5d(j = 3/2)$ orbitals, corresponding to t_{2g} orbitals, is higher than that of the $5d(j = 5/2)$ orbitals. The Γ_7 orbitals point along the ⟨111⟩ direction, where B_6 ligands exist. In the band structure of CeB_6, only $5d(e_g)$ orbitals corresponding to part of the $5d(j = 5/2)$ orbitals contribute to the hybridization with B-2p orbitals.

When both 5d orbitals were refined, the correlation between $n(5d_{j=5/2})$ and $n(5d_{j=3/2})$ was very strong. The correlation between the electron population of $2p_x$ (= $2p_y$) and the κ parameter of $2p_z$ also became severe. Thus, $n(5d_{j=5/2})$ or $n(5d_{j=3/2})$ was refined by fixing one of them at 0.0 and the κ parameters of the B-2p orbitals were also refined separately. When 5d orbitals are included in the analysis, the κ parameter of the Ce-5$p(j = 3/2)$ orbitals can be refined, in contrast to the analysis without 5d orbitals. The refinements (C) and (D), including the $5d(j = 5/2)$ and $5d(j = 3/2)$ orbitals, respectively, are listed in Table 2 and the corresponding residual densities around Ce are shown in Figs. 5(*a*) and (*b*). Since the residual densities around B are almost the same as those in Fig. 2(*d*), they are omitted. In Table 2, the R factors of the analyses, including $5d(j = 5/2)$ or $5d(j = 3/2)$, are evidently lower than those of the analysis without 5d orbitals. With respect to the analysis including $5d(j = 5/2)$, the peaks along the ⟨100⟩ direction of the residual density at 0.8 Å from Ce in Fig. 5(*a*) decreased significantly from 0.6 to 0.4 e Å^{-3}. This improvement is significant. When the analysis including $5d(j = 5/2)$ was performed, the $5d(j = 5/2)\Gamma_8$ orbitals were found to be fully occupied. From Table 2, the most significant result is the difference in populations of B-2p_x(= $2p_y$) between refinements (C), (D) and (B). A considerable number of electrons in the B-2p_x(= $2p_y$) orbitals are transferred to the Γ_8 orbitals of $5d(j = 5/2)$ or $5d(j = 3/2)$. $\kappa(2p_x)$ of B in refinement (B) is significantly smaller than that of $2p_z$ compared with refinements (C) and (D). Since the κ parameter and its error have a tendency to be larger when the parameter becomes smaller and *vice versa*, this may indicate that the population of B-2p_x (= $2p_y$) orbitals in refinement (B) is too large. However, in the present study the error of the κ parameter of B is large and the κ parameters are therefore less reliable. A comparison of the κ parameters of B-2p_x (= $2p_y$) orbitals and B-2p_z is not important. There is a difference between the κ parameter of B-2p_x (= $2p_y$) orbitals in refinements (B) and (C). However, this does not lead to the difference in population of B-2p_x (= $2p_y$) orbitals, since in refinement (C), before the κ parameter was refined, the population of B-2p_x (= $2p_y$) orbitals was 0.09 (6); after the κ refinement it was 0.10 (6). Thus, the correlation between the κ parameter of B-2p_x (= $2p_y$) and the population of B-2p_x (= $2p_y$) was not considered in refinement (C). The κ parameters of Ce are equal to one another in refinements (B)–(D), within experimental error. The electrons in B-2p_x (= $2p_y$) orbitals were reduced, but B-2p_z was not significantly affected by the refinements, as is evident from refinements (B)–(D) in Table 2.

The most important result of the present XAO analysis is the electron transfer from B_6 to Ce, and the inversion of the populations of the 4f-Γ_7 and 4f-Γ_8 orbitals of Ce. The latter was the lower energy state in our previous study at lower temperatures (Tanaka & Ōnuki, 2002). If the formal charges +3 and −0.5 for Ce and B, respectively, are assumed, the numbers of electrons transferred to Ce, which are calculated using the relation $6\{2(\frac{1}{2} - n(2p_x)) + (\frac{1}{2} - n(2p_z))\}$, are 0.30, 4.02 and 3.72 for refinements (B)–(D), respectively. Note that the number of electrons transferred from B in refinement (C) is equal to that of the $5d(j = 5/2)\Gamma_8$ orbitals, within experimental error, indicating that no electrons of the B-2p_x(= $2p_y$) orbitals are expected to be transferred to the 4f orbitals. The peaks in Fig. 2(*c*) were reduced after including $5d(j = 5/2)\Gamma_8$ orbitals in the refined parameters, as shown in Fig. 5(*a*). In refinement (D) $5d(j = 3/2)\Gamma_8$ orbitals are also fully occupied, as shown in Table 2. However, the peaks along the ⟨100⟩ direction of Ce in Fig. 5(*b*) show no improvement compared with those in Fig. 2(*c*). Moreover, the result of refinement (D) requires 0.28 (= 4–3.72) 4f electrons to be excited to 5d. Therefore, we conclude that $5d(j = 3/2)\Gamma_8$ orbitals are not occupied and refinement (C) gave the best results. Therefore, the residual peaks of Ce along the ⟨100⟩ direction with heights of 0.6 e Å^{-3} in Fig. 2(*c*) are concluded to be due to the electrons in $5d(j = 5/2)\Gamma_8$ orbitals. From equation (1) the ratio of $n(\Gamma_8)/n(\Gamma_7)$ is 0.16, indicating that energy levels of Γ_8 and Γ_7 are inverted with an energy gap of 783 K.

Since the energy level of the $5d(j = 3/2)\Gamma_8$ orbitals of Ce calculated by HEX is close to that of the 2p orbitals of B listed by Mann (1968), as illustrated in Fig. 4(*a*), the B-2p electrons are expected to be transferred predominantly to $5d(j = 3/2)\Gamma_8$ orbitals, according to the first-order perturbation theory. In addition, electron lobes of the B-2p_x(= $2p_y$) orbitals are located close to those of the 5d orbitals. Then electrons are transferred from $5d(j = 3/2)\Gamma_8$ orbitals to $5d(j = 5/2)\Gamma_8$ orbitals, since the transition from $5d(j = 3/2)\Gamma_8$ to $5d(j = 5/2)\Gamma_8$ is symmetry-allowed and the probability of the transition is expected to be higher than to the other orbitals. From Table

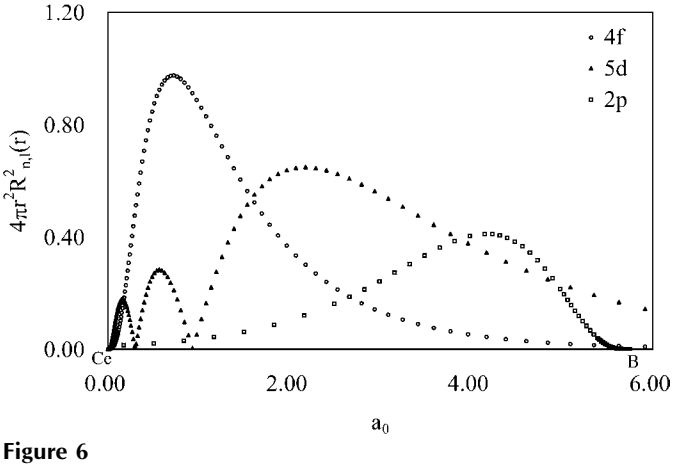

Figure 6
Radial distribution function of Ce-4f orbitals, 5d orbitals and B-2p orbitals.

2(*c*), the transfer of electrons from B-2p_x(= 2p_y) orbitals to Ce-5*d* orbitals is obvious. The radial distribution functions of 4*f* and 5*d* of Ce, and B-2*p* orbitals are illustrated in Fig. 6, and the EDD of Ce-4*f* and 5*d* orbitals in Fig. 7. Since the bond length between B and Ce is 3.045 Å (= 5.755 bohr), the B atom was placed at 5.755 bohr on the abscissa. The very strong overlap of the B-2*p* orbital and Ce-5*d* is easily understood. A filled 5*d*(j = 5/2)Γ_8 orbital is located outside the 4*f* orbitals and both have the same Γ_8 symmetry, with the EDD extending to the same directions. 4*f* orbitals are expected to be influenced by the 5*d* orbitals effectively. Therefore, the energy level of the 4*f*(j = 5/2)Γ_8 orbitals becomes higher than that of 4*f*(j = 5/2)Γ_7 because the electrostatic repulsion between electrons on 5*d*(j = 5/2)Γ_8 and 4*f*(j = 5/2)Γ_8 is larger than that between 5*d*(j = 5/2)Γ_8 and 4*f*(j = 5/2)Γ_7 orbitals. These electron transfers are illustrated in Fig. 4(*b*) by arrows.

5. Reliability of the result

The *R* factors of the refinements given in Table 2 are very close to one another. Furthermore, the numbers of parameters used in the refinements are different. Thus, it is necessary to judge the validity of the refinements. Using Hamilton's significance test (Hamilton, 1965), which may be valid for the evaluation of the analysis of electronic structure, the R_1(refinement(A))/R_1(refinement(C)) ratio is 1.083. This satisfied the significant level α = 0.05 ($R_{13,151,0.05}$ = 1.075) if insignificant AHV parameters are not taken into account, although the *R*-factor ratio for refinement (A)/(B) is not significant. Hence, refinement (A) without 5*d*(j = 5/2)Γ_8 orbitals is rejected at the 0.05 significance level. However, since the ratio of the number of *f* electrons to the total number of the electrons in the unit cell is very small, as stated in §2, the investigation of the EDD of rare-earth complexes needed great care and highly accurate measurement of the parameter interaction in the least-squares refinement. Since the smaller non-spherical EDD of the *f*-electrons reduces the *R* factor after the spherical-atom refinement (by 0.0125 in the present study), and since the two-center electrons are not considered in the present refinement, no further refinements could be made in the present study. Therefore, the reduction of *R* factors is not a good measure of the validity of the refinement, but the reduction of the peaks in the residual density maps should be noted. It sometimes happened that the residual density of Ce became higher when *R* values were reduced. Thus, the refinement was carried out while paying keen attention to the residual density around Ce, as well as the *R* values. However, the reduction of the numerator of the weighted *R* factor was also checked. Comparing the peak heights in Figs. 2(*a*) and 6(*a*) after refinements (A) and (C), respectively, the reduction of the peak on Ce from 0.8 to 0.2 e Å^{-3} and the 5*d* peaks from 0.6 to 0.4 e Å^{-3} can be seen, as described in §4.2.2. The residual density including 5*d*(j = 5/2) orbitals in Fig. 5(*a*) is lower than that including the 5*d*(j = 3/2) orbitals in (*b*), as well as the *R* factors. Since both refinements have the same number of parameters, we determined that refinement (C) was better than refinement (D). In refinement (C) the *n* and κ parameters of the AOs in the complex showed values greater than their e.s.d.'s. These orbital parameters of Ce are almost three times larger than their errors; $n(2p_x)$ of B is only 1.5 times larger than the error, but is still significant. This is caused by the transfer of a large number of electrons from B-2p_x (= p_y) orbitals to Ce-5*d* orbitals, and the remaining population values become relatively smaller. Most of the AHV parameters are

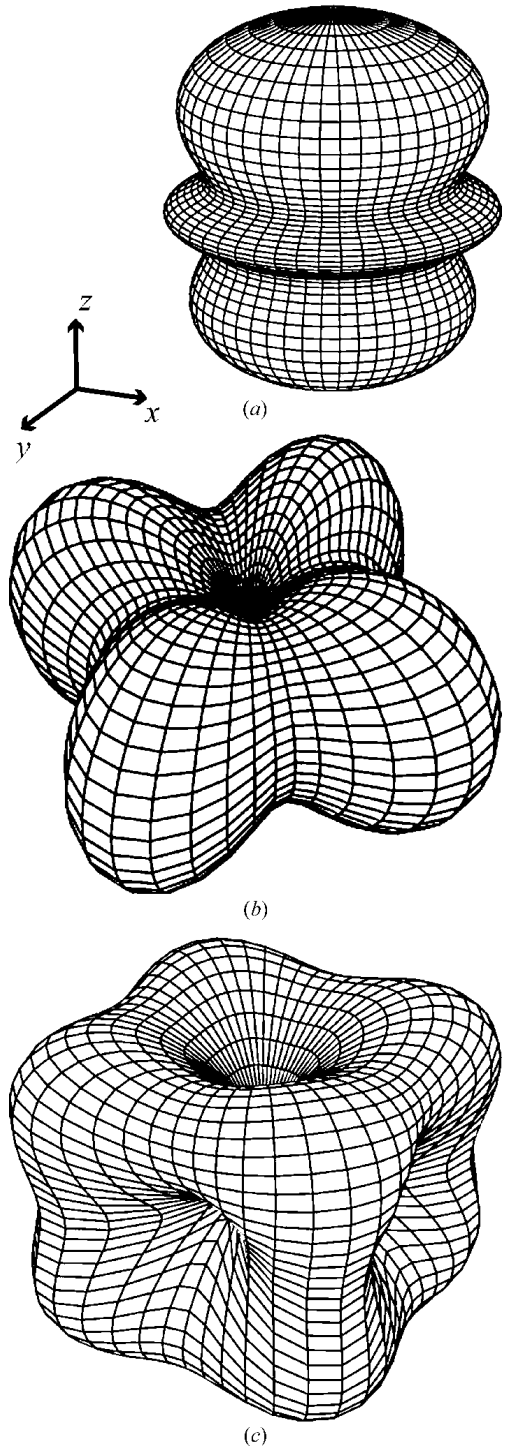

Figure 7
Schematic drawing of the electron densities of j = 5/2 orbitals of 4*f* and 5*d* (*a*) and (*b*) with the Γ_8 symmetry, and (*c*) with the Γ_7 symmetry.

insignificant because the AHV effect is small in CeB_6 at 430 K, as explained in §4.

Since the XAO analysis is based on the AOs which strictly obey the orthonormal relationships among them, and the fact that each orbital is not permitted to accommodate more electrons than those permitted by quantum mechanics, the population of each atomic orbital is more reliable than those obtained by other methods where no quantum-mechanical constraints are applied. This is the reason why self-consistent results, that is, fully occupied $5d(j = 5/2)\Gamma_8$ orbitals, which made the $4f$ orbital with the same symmetry property ($j = 5/2,\Gamma_8$) unstable, resulting in the inversion of the energy levels and the electron populations, were obtained in the present study. The XAO analysis does not take into account the two-centre electrons, as seen in Figs. 2(*b*) and (*d*), where the EDD on the centre of the B—B bond is not affected by the refinements mthods. The introduction of MOs is necessary to account for the EDD of the B—B bonds.

The multiple diffraction effect becomes very large in rare-earth complexes, since the effect is proportional to the square of the structure factors (Moon & Shull, 1964). Thus, it easily becomes one or two orders higher than those of the organic compounds. Although Claiser *et al.* (2004) pointed out that the scattering factors were not good enough to observe the EDD of rare-earth complexes, avoidance of the multiple diffraction effect was essentially important in the present study. The use of synchrotron radiation is expected to reduce this effect because the small beam divergence of the incident synchrotron radiation beam reduces the chances of the effect occurring. However, when the half-width of the Bragg peak is large due to the mosaicity of the crystal, multiple diffraction becomes very significant even in the synchrotron radiation experiment (Komori *et al.*, 2007).

6. Conclusion

At 430 K, the X-ray diffracted intensity of CeB_6 was measured in order to observe the thermally excited EDD. A considerable number of electrons occupies the Γ_7 orbitals when electrons are transferred from B to Ce. We are confident that the EDD of thermally excited states of CeB_6 can be observed. The energy levels of $4f(j = 5/2)\Gamma_8$ and Γ_7 orbitals are inverted and the Γ_7 orbitals become the ground state. This is caused by the electron occupation of $5d(j = 5/2)\Gamma_8$ orbitals extending the electron lobes in exactly the same directions as $4f(j = 5/2)\Gamma_8$ orbitals. To confirm this phenomenon, further measurements of EDD at temperatures between 298 and 430 K and higher are necessary.

References

Becker, P. J. & Coppens, P. (1974*a*). *Acta Cryst.* A**30**, 129–147.
Becker, P. J. & Coppens, P. (1974*b*). *Acta Cryst.* A**30**, 148–153.
Becker, P. J. & Coppens, P. (1975). *Acta Cryst.* A**31**, 417–425.
Brown, G. E., Sueno, S. & Prewitt, C. T. (1973). *Am. Mineral.* **58**, 698–704.
Claiser, N., Souhassou, M. & Lecomte, C. (2004). *J. Phys. Chem. Solids*, **65**, 1927–1933.
Coppens, P., Guru Row, T. N., Leung, P., Stevens, E. D., Becker, P. J. & Yang, Y. W. (1979). *Acta Cryst.* A**35**, 63–72.
Dawson, B., Hurley, A. C. & Maslen, V. W. (1967). *Proc. R. Soc. London Ser. A*, **298**, 289–306.
Dyall, K. D., Grant, I. P., Johnson, C. T., Parpia, F. A. & Plummer, E. P. (1989). *Comput. Phys. Commun.* **55**, 425–256.
Hamilton, W. C. (1965). *Acta Cryst.* **18**, 502–510.
Heide, P. V. D., Cate, H. W. T., Dam, L. M. T., Groot, R. A. D. & Vroomen, A. R. D. (1986). *J. Phys. F Met. Phys.* **16**, 1617–1623.
Ichikawa, I., Nisawa, A. & Tsutsumi, K. (1986). *Phys. Rev. B*, **34**, 6690–6694.
Ishizawa, N. & Kato, M. (1983). *J. Mineral. Soc. Jpn*, **16**, Special Issue No. 1, 13–20.
Kakizaki, A., Harusawa, A., Ishii, T., Kashiwakura, T., Kamata, A. & Kunii, S. (1995). *J. Phys. Soc. Jpn*, **64**, 302–307.
Kim, C. D., Pillet, S., Wu, G., Fullagar, W. K. & Coppens, P. (2002). *Acta Cryst.* A**58**, 133–137.
Kodama, N. (1984). PhD thesis. Interdisciplinary Graduate School of Science and Engineering, Tokyo Institute of Technology.
Komori, T., Sakakura, T., Takenaka, Y. & Tanaka, K. (2007). To be published.
Liberman, D. A., Cormer, D. T. & Waber, J. T. (1971). *Comput. Phys. Commun.* **2**, 107–113.
Loewenhaupt, M., Carpenter, J. M. & Loong, C.-K. (1985). *J. Magn. Magn. Mater.* **52**, 245–249.
Mann, J. B. (1968). Report LA3691. Los Alamos National Laboratory, New Mexico, USA.
Martin, W. C., Zalubas, R. & Hagan, L. (1978). *Atomic Energy Levels – The Rare Earth Elements.* NSRDS-NBS, Washington: National Bureau of Standards, US Department of Commerce.
Moon, R. M. & Shull, C. G. (1964). *Acta Cryst.* **17**, 805–812.
Ozawa, Y., Terashima, M., Mitsumi, M., Toriumi, K., Yasuda, N., Uekusa, H. & Ohashi, Y. (2003). *Chem. Lett.* **32**, 62–63.
Pressprich, M. R., White, M. A., Vekhter, Y. & Coppens, P. (1994). *J. Am. Chem. Soc.* **116**, 5233–5238.
Sakurai, T. & Kobayashi, K. (1979). *Rep. Inst. Phys. Chem. Res.* **55**, 69–77.
Sato, S. (1985). *J. Magn. Magn. Mater.* **52**, 310–312.
Souma, S., Iida, Y., Sato, T., Takahashi, T. & Kunii, S. (2004). *Physica B*, **351**, 283–285.
Tanaka, K. (1988). *Acta Cryst.* A**44**, 1002–1008.
Tanaka, K., Kato,Y. & Ōnuki, Y. (1997). *Acta Cryst.* B**53**, 143–152.
Tanaka, K., Kumazawa, S., Tsubokawa, M., Maruno, S. & Shirotani, I. (1994). *Acta Cryst.* A**50**, 246–252.
Tanaka, K., Makita, R., Funahashi, S. & Komori, T. (2007). *Acta Cryst.* To be submitted.
Tanaka, K. & Marumo, F. (1983). *Acta Cryst.* A**39**, 631–641.
Tanaka, K. & Ōnuki, Y. (2002). *Acta Cryst.* B**58**, 423–436.
Thornley, F. R. & Nelmes, R. J. (1974). *Acta Cryst.* A**30**, 748–757.
Weiss, R. J. & Freeman, A. J. (1959). *J. Chem. Phys. Chem. Solids*, **10**, 147–161.
Zirngiebl, E., Hillerbrands, B., Blumenroder, S., Guntherodt, G., Loewenhaupt, M., Carpenter, J. M., Winzer, K. & Fisk, Z. (1984). *Phys. Rev. B*, **30**, 4052–4054.